Comparison of CO_2-Brine and N_2-Brine Relative Permeability on Multiple Rock Types Using Physical and Digital Rock Analysis Methods

Melissa Martin[1,*], *Michael* Suhrer[3], *Stephen* Drylie[1], *Feiyan* Chen[1], *Phillip* Mendoza[3], *Birol* Dindoruk[2], *David* Gonzalez[3], *Gustavo* Carpio[3]

[1]Core Laboratories, Petroleum Services, 6316 Windfern Rd. Houston, TX, U.S.A.
[2]Texas A&M University, Harold Vance Department of Petroleum Engineering, 801A Richardson Building 3116 TAMU, College Station, TX, U.S.A.
[3]Halliburton, Wireline & Perforating, 3000 N. Sam Houston Pkwy E. Houston, TX, U.S.A.

Abstract. Carbon storage projects require both reservoir characterization and reservoir modelling to adequately describe the reservoir. One key component to both requirements is relative permeability data. However, CO_2-Brine relative permeability testing has proven to be challenging in the laboratory, often resulting in extended testing time, increased cost, and limited experimental data. To address these challenges, alternative testing approaches, fluid pairs, and digital rock analysis workflows were evaluated and compared with the aim of simplifying relative permeability characterization while reducing time and cost. While there are numerous studies to compare methods for acquiring relative permeability data in conventional systems, detailed comparisons for CO_2 systems remain limited. This work addresses that gap by integrating laboratory measurements with digital rock analysis to evaluate multiple testing methods and fluid pairs that may permit more efficient and extensive relative permeability characterization for carbon capture and storage projects.

1 Background

The work described in this paper is part of a broader study investigating important considerations for CO_2 sequestration. Initial research efforts focused on evaluating seal properties and methods for determining entry pressures. As part of this effort, samples from multiple CCUS reservoir seals and one proxy formation were exposed to CO_2 saturated brine at 150°F and 1500 psi for periods of one, three, and six months. Various diagnostic methods were employed including thin section description and high-pressure mercury injection with little evidence of significant rock property change even in carbonate dominated formations [1].

In the following year, the focus shifted to the study of CO_2 exposure under flowing conditions and continued static exposure in injection zones. An organized and detailed testing and characterization sequence was carried out on 12 quarry rock groups anchored by a retained permeability type test after 5 days of CO_2 saturated-brine (i.e. the reactive fluid) flow. Both rock and fluids from the test were evaluated for changes resulting from this flow with significant and variable changes seen depending on the rock being exposed. This is a stark contrast to the limited reactivity seen with the less permeable seals under static exposure. Sandstone type formations typically showed reduction in permeability resulting from a combination of reactivity and fines migration. Carbonates typically showed increased permeability resulting from wormhole development. Full results have been published separately [1].

The research highlighted in this paper examines relative permeability relationships in CO_2-brine systems and compares them with those observed in nitrogen-brine systems. Relative permeability measurements have always been challenging due to required measurement precision, sensitivity to sample variability both before and during testing, and uncertainty related to simulating reservoir dynamics. The introduction of reactivity inherent in any system containing CO_2 complicates the testing further. Flow conditions at reservoir conditions are often within the supercritical envelope of CO_2 changing the physical properties and potentially flow behavior especially when compared against nitrogen or typical hydrocarbons that remain in the gaseous phase. The goal of this study was to isolate the various factors governing flow dynamics through digital solutions and testing under controlled variable conditions allowing testing assumptions to be verified. This verification can provide confidence to operators and regulators that reservoir

* Corresponding author: melissa.martin@corelab.com

models properly account for the unique mechanisms governing CO_2 flow under super critical conditions while simultaneously allowing for the optimal testing protocol to be selected with full recognition of uncertainties and risks.

2 Samples

To ensure consistent material across all tests, quarry rock samples were utilized in this study. The full program, incorporated rocks from twelve different formations, consisting of both sandstones and carbonates, with Klinkenberg permeability ranging from 6.17 to 1125 millidarcies and porosities ranging from 10.9 to 42.9%.

For the dynamic injection relative permeability study, only sandstone samples were selected for unsteady state relative permeability testing: Nugget, Bentheimer, and Bandera Brown. Additionally, Berea sandstone was evaluated through centrifuge relative permeability testing and digital rock analysis. The permeability to air ranged from 1.89 to 2670 millidarcies, with porosities ranging from 12.5 to 22.9%, see *Fehler! Verweisquelle konnte nicht gefunden werden.*.

Nugget sandstone, Figure 1 is an upper-medium grained sandstone consisting of 90.7% quartz with a total clay amount of 3.8%.

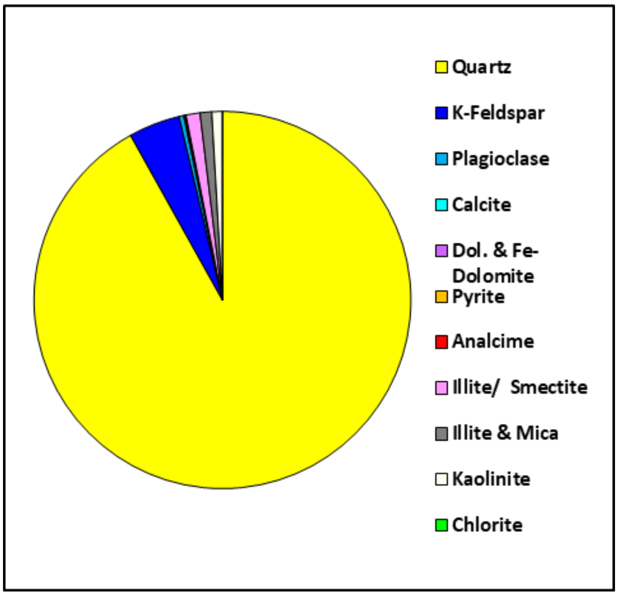

Figure 1: Nugget Sandstone Mineralogy

Bentheimer Sandstone, Figure 2, is a medium grained sandstone consisting of 96.5% quarts with a total clay amount of 1.0%

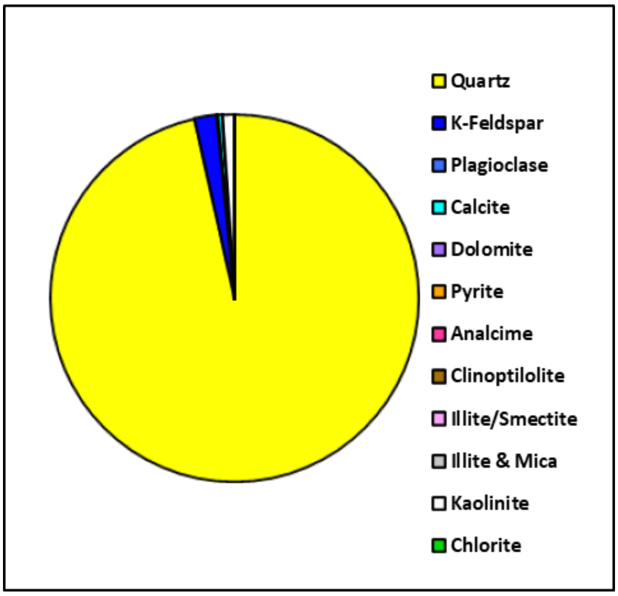

Figure 2: Bentheimer Sandstone Mineralogy

Bandera Brown, Figure 3, Sandstone is an upper very fine-grained sandstone consisting of 65% quartz with a total clay amount of 17%.

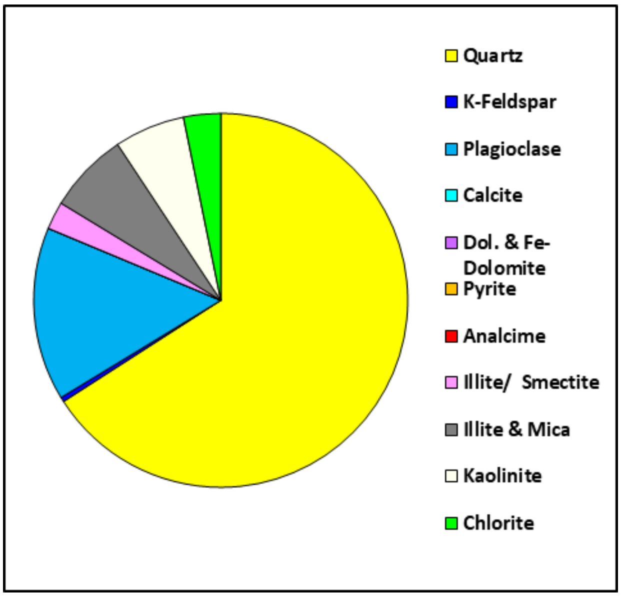

Figure 3: Bandera Brown Sandstone Mineralogy

Table 1: Relative Permeability Study Routine Core Properties

Sample Number	Porosity (%)	Permeability Klinkenberg (md)	Permeability Kair (md)	Grain Density (g/cm3)	Length (cm)	Diameter (cm)
23a-Nugget	12.53	152	157	2.639	6.725	3.783
62b-Bande	15.05	1.43	1.89	2.702	6.630	3.768
1-Bentheim	22.95	NA	2670	2.638	27.883	3.801
2-Bentheim	22.54	NA	2630	2.635	27.803	3.799

Berea Sandstone, Figure 4, is an upper fine-grained sandstone consisting of 85.4% quartz with a total clay amount of 7.2%.

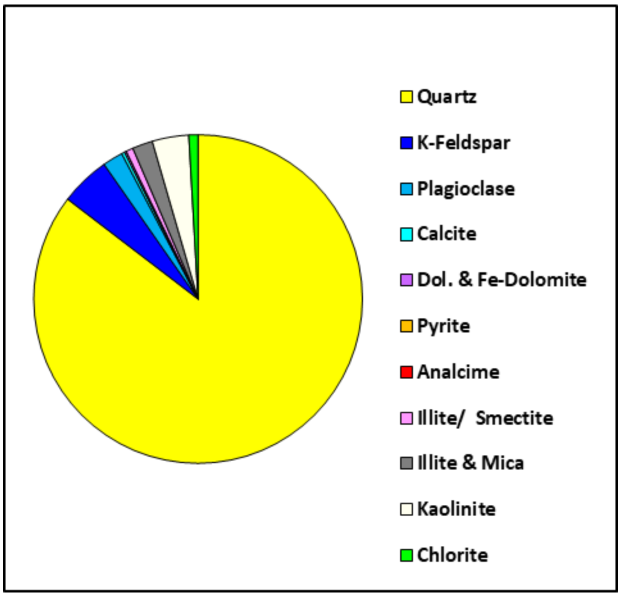

Figure 4: Berea Sandstone Mineralogy

3 Methodology

3.1 Dynamic Relative Permeability

Relative permeability testing was carried out in four phases to ensure a comprehensive evaluation. Phase I consisted of sample screening, selection, and preparation. Phase II focused on unsteady-state drainage relative permeability measurements using both nitrogen-brine and CO_2-brine fluid systems. Phase III applied Brooks-Corey modelling from capillary pressure data [2,3]. Phase IV incorporated digital rock evaluation for further characterization.

3.1.1 Sample Screening, Selection, and Preparation

Phase I involved selecting multiple samples of each rock type for initial screening. Each sample underwent Micro-CT imaging to obtain a non-destructive internal characterization. The resulting images were analyzed to confirm consistency among samples from the same lithology. In addition, the images were analyzed for any internal features, such as fractures, that would compromise structural integrity or otherwise affect relative permeability results.

Selected samples were trimmed to right cylinders and the trims retained for digital rock evaluation. All samples were cleaned with chloroform methanol azeotrope followed by methanol using a refluxing Soxhlet Apparatus. Cleaning was considered complete once the solvent was visually clear and methanol did not precipitate silver nitrate ($AgNO_3$). Samples were then dried to a constant weight using a 140°F convection oven. Finally, routine core properties were measured.

3.1.2: Unsteady-State Primary Drainage Relative Permeability

Unsteady-state drainage relative permeability was performed using both nitrogen-brine and CO_2-brine fluid systems. Originally, the program was designed to perform relative permeability testing for all fluid systems on the same sample. However, due to fines migration concerns encountered on nugget samples, the program was redesigned for bentheimer, bandera brown, and berea sandstones: to use similar but separate samples for each fluid system.

To perform the testing, each selected sample was received by the laboratory. cleaned, dried, and routine core properties measured. Each sample was saturated to 100% water saturation (Sw) with 10^5 ppm (80:20 NaCl:KCl) brine using a vacuum/pressure saturation method. The saturated sample was then loaded into the relative permeability system at the appropriate testing condition. Testing conditions were kept similar for each testing variation across the rock type. The testing conditions are as follows:

Table 2: USS Relative Permeability Testing Conditions

Fluid Pair (Graph Label)	Net Confining Stress (NCS) (psi)	Test Temperature (F)	Pore Pressure (psi)
Nitrogen-Brine (Amb N2)	1000	Ambient	200
Nitrogen-Brine (EL-N2)	1000	150	1500
CO_2-Brine (SC-CO_2)	1000	150	1500

The brine saturated sample was loaded into the testing system, and the appropriate testing conditions were applied, see Table 2. For both Nitrogen-brine tests, dead brine and humidified nitrogen were used. For the CO_2-Brine test at 150°F and 1500 psi, CO_2-saturated brine and brine-saturated CO_2 were used.

The relative permeability testing was performed using the unsteady-state method. A capillary number ranging from 10E-07 to 10E-08 was used for all tests. Nitrogen, or CO_2, was injected vertically downward through each sample at a constant rate to displace the brine. Differential pressure, produced volumes, and elapsed time were recorded until brine production ceased. Effective permeability to gas at residual water saturation (Swr) was determined. Two bump rates were performed by increasing the gas rate. Effective permeability to gas at Swr was determined at each bump rate.

For two samples, Nugget and Berea, unsteady-state centrifuge was also performed using a decane-displacing-brine fluid system.

Post test, the sample and system were returned to ambient conditions while monitoring any additional brine production. Dean-Stark evaluation was performed to confirm final saturations.

USS Relative Permeability was evaluated using the methods defined by Jones-Roszelle. Final effective permeabilities were determined using Darcy's Law. In addition, history matching simulation was performed. Results can be found in Appendix B.

3.1.3: Primary Imbibition by Counter Current Imbibition (CCI)

Imbibition was not the primary focus of this study. However, trapped gas saturation was evaluated using the CCI method. Results can be found in Appendix A.

3.2 Relative Permeability Evaluation by Digital Rock Analysis (DRA Model)

Digital rock analysis (DRA) was performed on 3 plugs: Nugget, Berea, and Bentheimer. The plugs used for DRA are from the same formation, but not the same plugs used for the remainder of the study. They were received cleaned and dried. CT volumes are first generated for the whole plug to select representative locations for extracting micro plugs to scan at a higher resolution where porosity can be directly imaged and segmented. Next, absolute permeability trends and capillary pressure curves are simulated and compared against laboratory data to ensure the samples are representative and cover the effective pore space responsible for fluid flow. Relative permeability curves are then simulated.

Interfacial tension and contact angles were estimated from literature. Overall IFT trends are consistent, however there is dispersion in reported contact angle statistics due to differences in substrate types, preparation methods, surface roughness values, and pattern [4-11]. The fluid properties used for both drainage and imbibition cycles are shown in Table *3*.

Table 3: Fluid properties used for DRA simulations. These properties are used for both drainage and imbibition cycles.

Interfacial Tension	30 dynes/cm
Contact Angle	30°
Water Viscosity	0.56 cP
CO_2 Viscosity	0.024 cP

3.2.1 Multi-scale X-Ray CT imaging and segmentation

Each plug is first scanned at low resolution, in this case 40 microns/voxel and evaluated for heterogeneities. A representative location is selected, and a smaller micro-pillar is milled to scan at a higher resolution, in this case 2 µm/voxel for all 3 samples. The volumes and their respective locations/sizes are shown in Figure 5. Berea and Bentheimer are both homogeneous at the plug scale; a single 2,000 x 2,000 x 2,000 voxel scan of a micro plug 4 mm in diameter is sufficient to characterize the plugs. Nugget is highly laminated; a 4,000 x 4,000 x 4,000 voxel scan of a micro plug 8 mm in diameter is necessary to capture a representative volume. The resulting volumes are then segmented into pore and various mineral phases using a watershed-based segmentation approach [12].

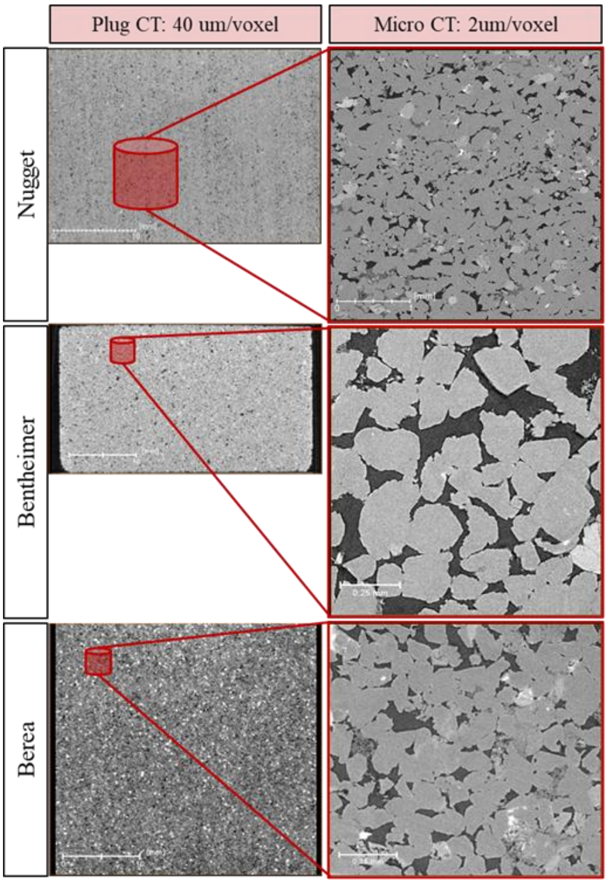

Figure 5: CT images of each plug at a resolution of 40 um (left) and each extracted micro-plug at a resolution of 2 um (right). The size and location of each micro-plug is indicated by the red cylinder.

3.2.2 Permeability Trends

Porosity is determined directly from the segmented volumes at a resolution of 2µm/voxel where pore space is resolved. Permeability is computed from numerical flow simulations using the lattice Boltzmann method [13]. This is performed on a multitude of randomly distributed cubes from within the segmented volume, generating a functional relationship, trend, between porosity and absolute permeability. To ensure the results are representative, the size of the cube is determined using the local porosity theory to select a representative elementary volume [14]. The DRA trends are shown in Figure 6 along with the full volume containing the cubes and helium porosity/permeability measurements on the entire plug. The trends agree with helium porosity/permeability measurements with a net confining stress of 2,000 psig.

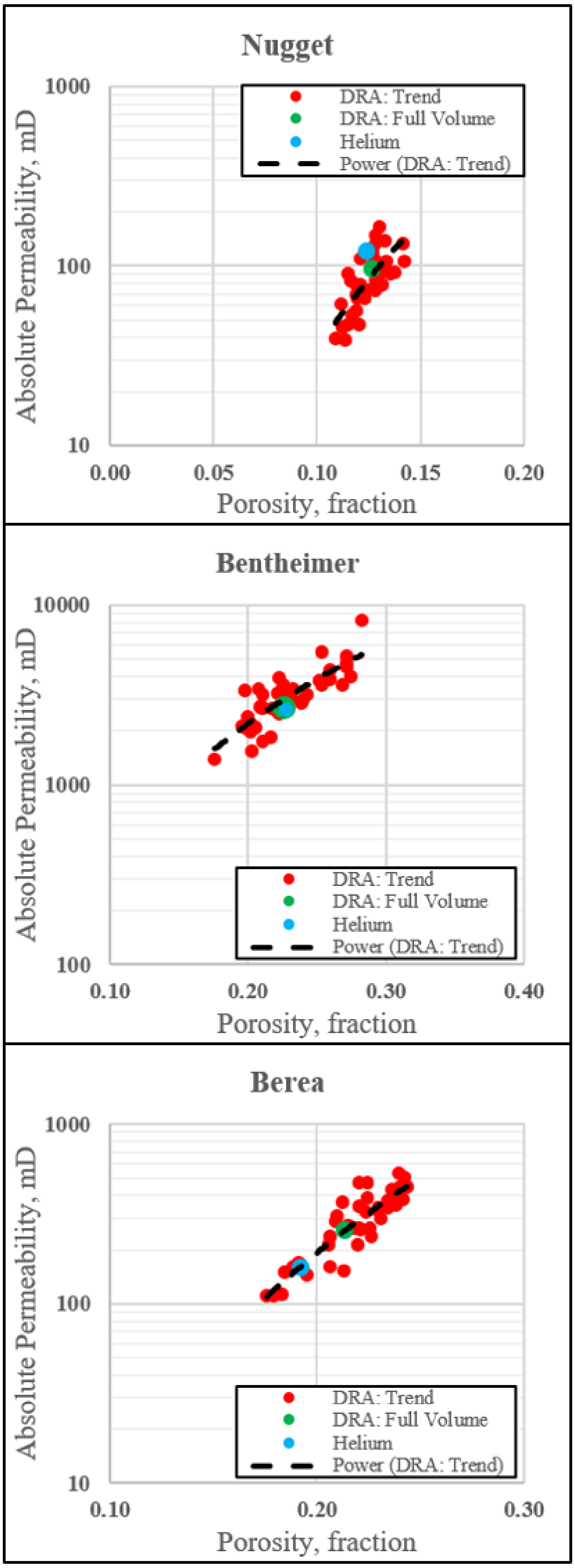

Figure 6: Digital permeability trends (red) for each sample. The trends agree with helium porosity/permeability results (blue).

3.2.3 Capillary Pressure

Capillary pressure curves, drainage and imbibition, are computed on the resolved pore space in the 2µm/voxel resolution segmented volumes using a lattice Boltzmann based simulator developed for the task [15]. MICP data is scaled to the fluid properties used for the DRA simulations and compared against primary drainage to verify the volume is representative. The capillary pressure curves are shown in Figure 7. The primary drainage curves are a reasonable match to MICP for each sample and cover the effective pore space responsible for fluid flow. The microporosity is considered to remain water saturated.

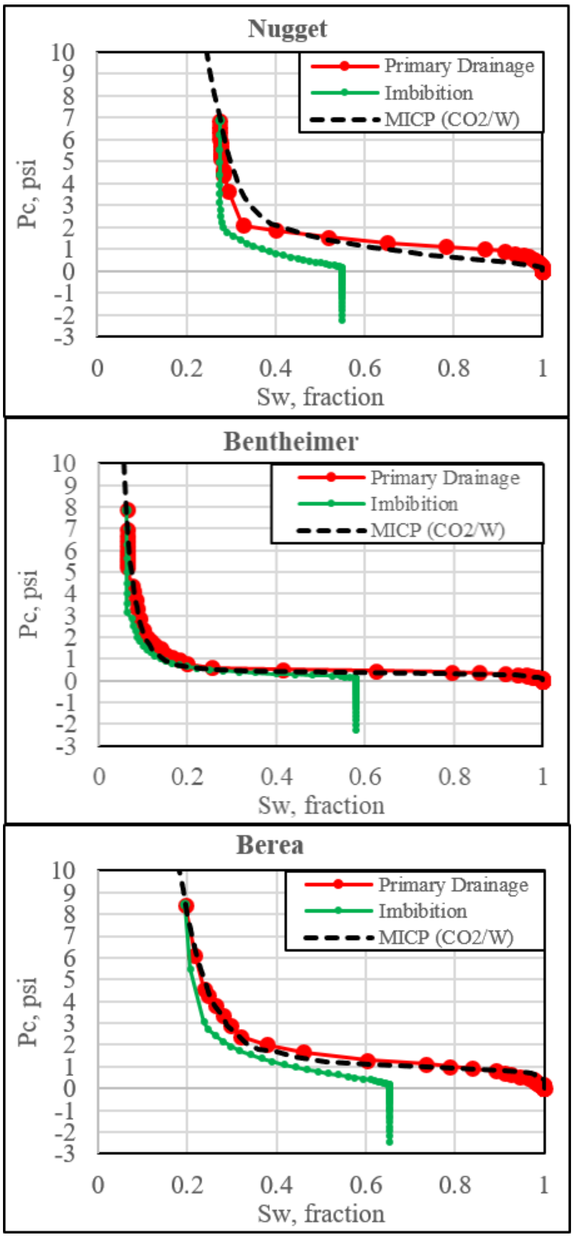

Figure 7: Digital primary drainage (red) and imbibition curves (green) for each sample. The drainage curves are a reasonable match with MICP (black) scaled to the fluid properties used for DRA simulations.

3.2.4 Relative Permeability

Relative permeability curves, drainage and imbibition, are computed on the resolved pore space in the 2µm/voxel resolution segmented volumes using a steady-state simulator developed for the task [16]. Simulations are performed at a low capillary number to avoid undesirable viscous flow effects. Relative permeability curves for each sample are shown in Figures 8–10. The residual CO_2 values agree with what is expected from strongly water wet samples with initial water saturations (Swi) between 0.0 and 0.4 Sw [17].

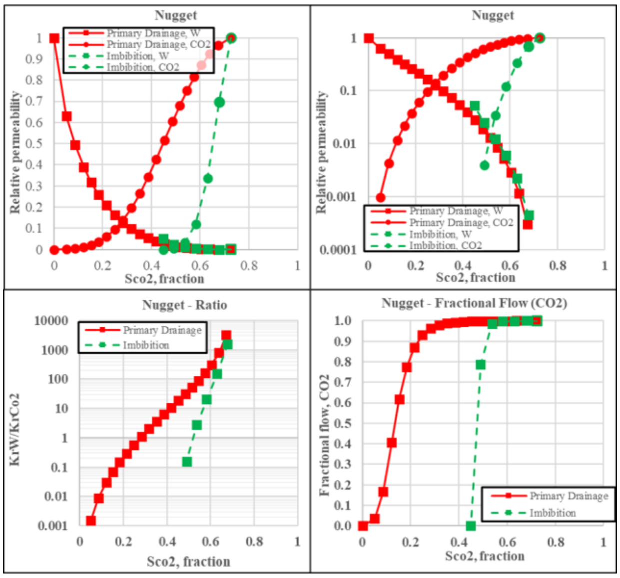

Figure 8: DRA drainage (red) and imbibition (green) relative permeability curves for Nugget sandstone.

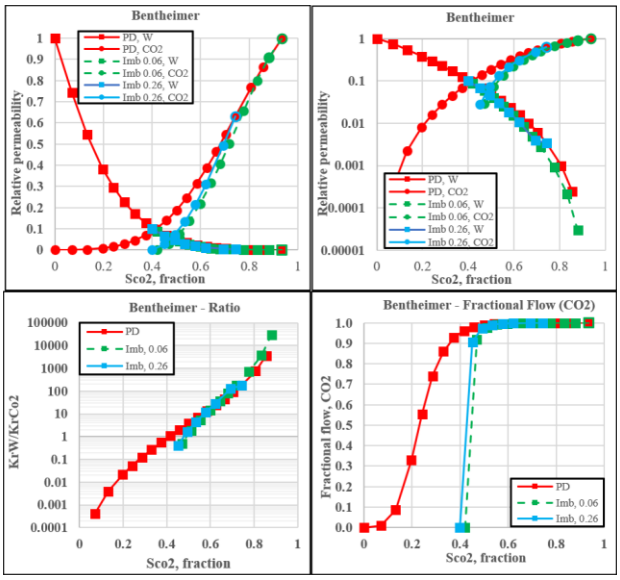

Figure 9: DRA drainage (red), imbibition starting at Swi = 0.06 (green), and imbibition starting at Swi = 0.26 (blue) relative permeability curves for Bentheimer sandstone.

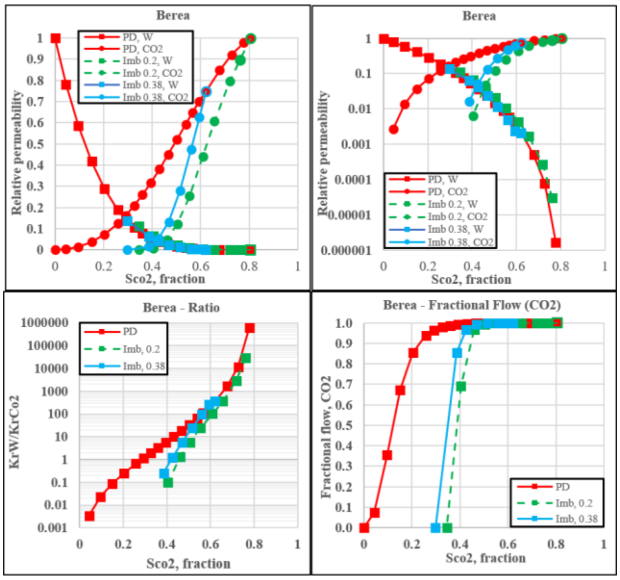

Figure 10: DRA drainage (red), imbibition starting at Swi = 0.20 (green), and imbibition starting at Swi = 0.38 (blue) relative permeability curves for Berea sandstone.

4 Results

To develop relative permeability data across the full saturation range, three evaluation approaches were applied: dynamic injection testing, Brooks–Corey modeling derived from capillary-pressure measurements, and digital rock analysis. Each method was evaluated independently, and the resulting data sets were then compared to determine consistency and identify key differences.

4.1 Nugget Sandstone

Physical results from the nugget sandstone tests along with curve fits are shown in Figure 11 below. Before interpreting the match between the three datasets, it is important to note that this sample showed strong evidence of fines migration during testing. Permeability showed consistent drops during testing without a change in fluid saturation. Additionally, thin section and SEM (Scanning Electron Microscopy) analysis performed at the end of testing revealed areas where fines (Kaolinite) were unnaturally oriented, showed evidence of redistribution, and occluding pore throats, see Figures 12-14. By referencing all effective permeabilities back to the permeability at the start of that fluid pair, effective permeability trends can be compared, and similarities noted. Due to fines migration potential, the program was redesigned for Bentheimer, Bandera brown, and Berea sandstones utilizing separate but similar samples for relative permeability tests with each fluid pair. Overall, all three datasets align closely although the ambient nitrogen test could not achieve the same final gas saturation. Slight differences in curve shape of the effective permeability to gas can be noted especially for the nitrogen at elevated temperature, but effective permeability to water shows consistent trends apart from the above noted difference in endpoint.

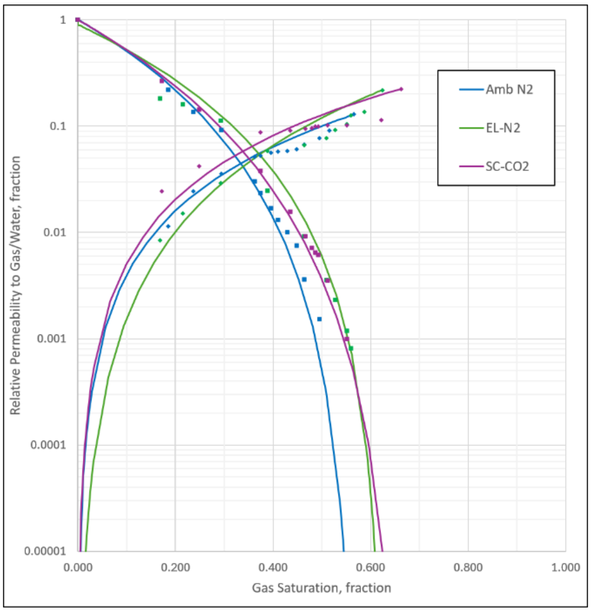

Figure 111: Nugget Sandstone Relative Permeability Results from Dynamic Injection Testing

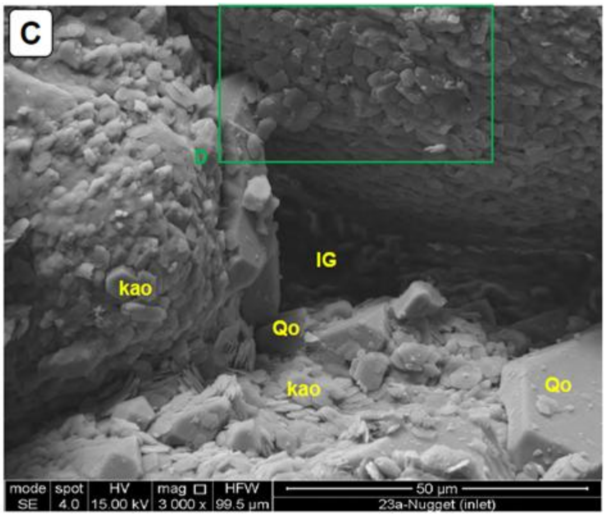

Figure 122: SEM (Scanning Electron Microscopy) Image of Nugget Sandstone Inlet Face Trim, Post Relative Permeability Testing Showing Unnaturally Oriented Platelets. Kao (Kaolinite), IG (Intergranular), Qo (Quartz overgrowth)

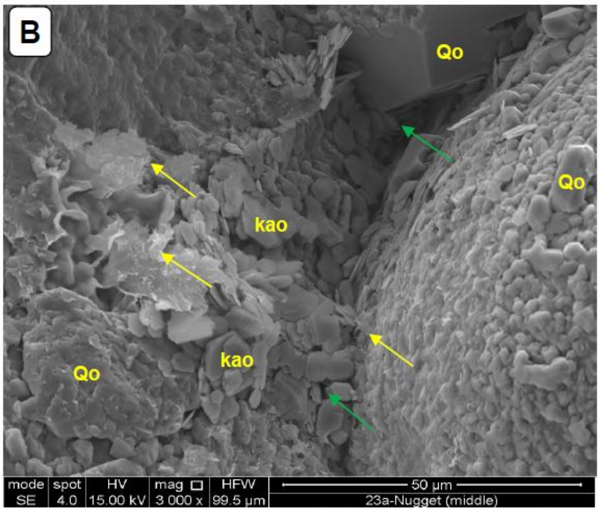

Figure 133: SEM (Scanning Electron Microscopy) Image of Nugget Sandstone Middle Trim, Post Relative Permeability Testing Showing Unnaturally Oriented Platelets. Kao (Kaolinite), Qo (Quartz overgrowth)

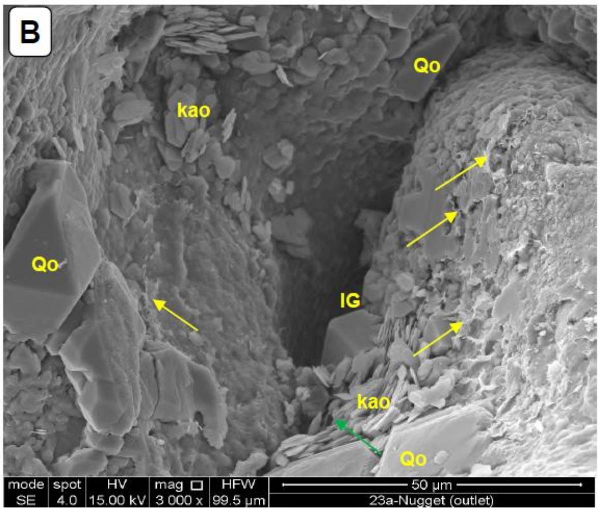

Figure 144: SEM (Scanning Electron Microscopy) Image of Nugget Sandstone Outlet Face, Post Relative Permeability Testing Showing Unnaturally Oriented Platelets. Kao (Kaolinite), IG (Intergranular), Qo (Quartz overgrowth)

Figure 15 adds a Corey model fit for all three tests. Using a model fit removes the flattening of effective gas saturation seen in all three tests above a gas saturation of approximately 0.4. This behavior is seen in many tests of high permeability samples and is suspected to result from gas bypassing much of the pore space once a continuous path through the sample has been achieved. Bump rates can correct some of this streamlining, but pressure drop is insufficient in this system to fully incorporate the pore space. DRA simulations are run at low capillary numbers to avoid viscous flow effects such as viscous fingering and therefore do not show flattening of the gas curve. Otherwise, the data consistency between test types is maintained except that the notable outlier in curve shape is the effective permeability to supercritical CO_2.

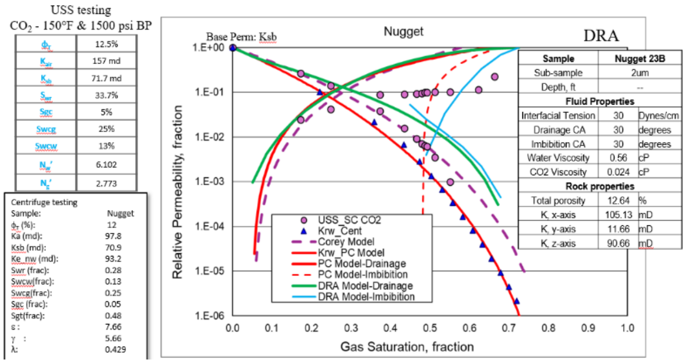

Figure 15: Nugget Sandstone Combined Relative Permeability Data

4.2 Bentheimer Sandstone

Testing in Bentheimer Sandstone removed the nitrogen test at ambient conditions and used a different plug for each fluid to reduce the uncertainty resulting from fines migration. This change does introduce uncertainty related to variability between the plugs which was addressed through careful sample selection guided by µCT scanning and routine property measurement. The match between the two fluids is even stronger for this rock type resulting in the two datasets and matched curves overlapping as shown in Figure 16.

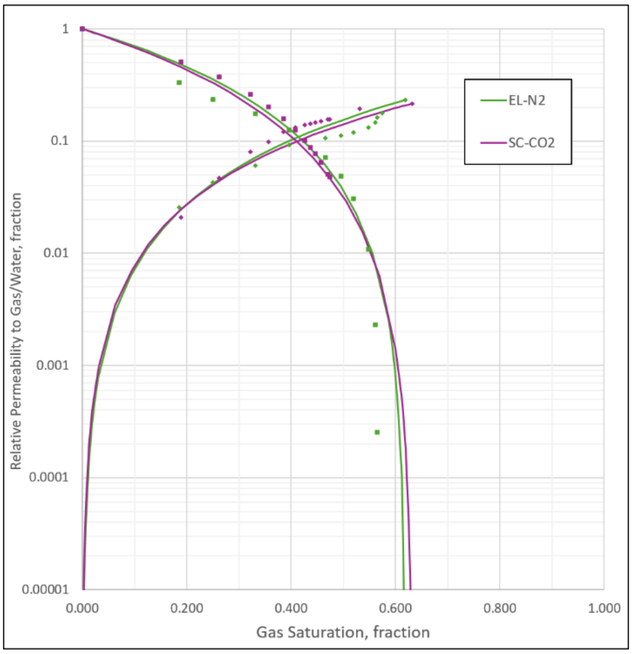

Figure 16: Bentheimer Sandstone Relative Permeability Results from Dynamic Injection Testing

Figure 17 shows a comparison of the super critical CO_2 data and various models for permeability. All four methods yield similar results apart from a slight difference in curve shape seen in the relative permeability to CO_2 predicted by the Corey model. This rock also showed less flattening of the relative permeability curve as a result of bypassed pore space.

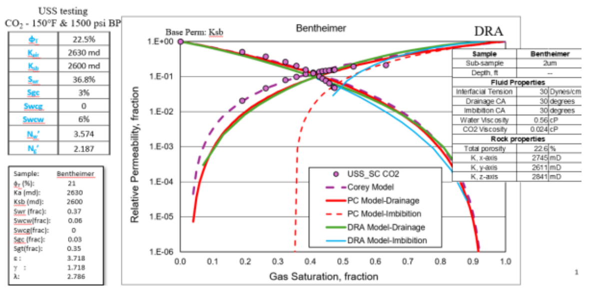

Figure 17: Bentheimer Sandstone Combined Relative Permeability Data

4.3 Bandera Brown Sandstone

Bandera Brown testing showed a poorer match between the two fluid types. Even the saturation range over which effective permeability could be measured was not consistent. This could have resulted from heterogeneity between the test samples.

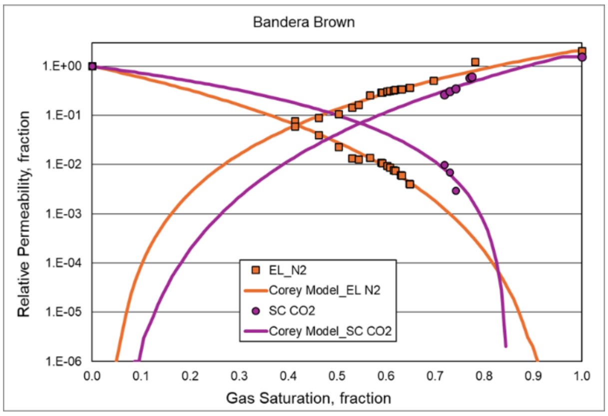

Figure 18: Bandera Brown Combined Relative Permeability Data

4.4 Berea Sandstone

Dynamic testing on Berea Sandstone was limited to decane-brine centrifuge relative permeability measurement. This measurement technique only provides data for the displaced fluid, brine, as is seen in Figure 19 below. A Brooks-Corey fit using capillary pressure data matched these data points well although the digital model showed a noticeable difference in curve shape.

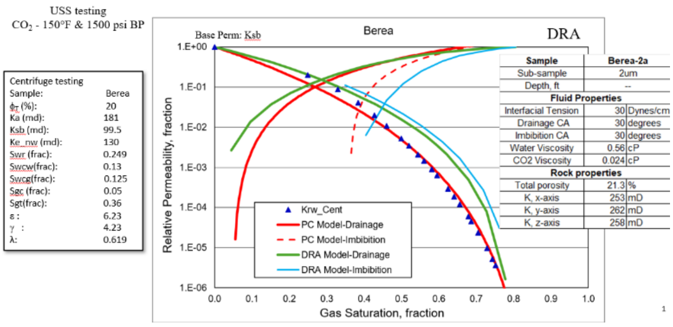

Figure 19: Berea Sandstone Combined Relative Permeability Data

5 Conclusions

CO_2 Relative Permeability testing has known challenges that must be overcome to enable CCUS project planning and authorization. This paper compares several options for gathering this critical data and validating their use to regulatory bodies.

- Testing with nitrogen can yield comparable results to supercritical CO_2 especially if temperature and pressure conditions are aligned although this behavior may be limited to drainage on the water wet clean sands tested.
- Laboratory testing with any high-permeability, low-pressure drop system can result in inefficient displacement of the higher viscosity fluid. This can be compounded by the lower than ideal capillary number associated with low viscosity fluids and flow rate limitations.
- DRA simulations are run at low capillary numbers to avoid viscous flow effects such as viscous fingering and can be used in high-permeability low-pressure drop systems without suffering from inefficient displacement of the high viscosity phase.
- Enhancement of laboratory results with empirical models or digital flow simulation can yield more theoretically expected relative permeability curves.
- Additional outputs within digital rock models can provide insight into further dynamics of flow and implications of endpoints and rock-fluid or fluid/fluid interactions.
- The DRA model does not allow for the movement of solid material during simulations and can mitigate the issue of fines migration affecting results.
- Combining multiple analysis types can reduce both uncertainty and risk in CCUS projects.

References

1. M. Martin, S. Drylie, J. Antia, F. Chen, J. Green, B. Dindoruk, Formation Damage Concerns and Laboratory Considerations with CO_2 Injection in Carbon Storage Wells, *SPE International Conference & Exhibition on Formation Damage Control*, Lafayette, Louisiana, USA, (18-20 February 2026)
2. M. B. Standing, Notes on relative permeability relationships: Division of Petroleum Engineering and Applied Geophysics, Norwegian Institute of Technology, University of Trondheim, Norway (1974)
3. C. S. Land, Comparison of Calculated with Experimental Imbibition Relative Permeability, *SPE J.* (1971)
4. P. Chiquet, J. L. Daridon, D. Broseta & S. Thibeau, CO2/water interfacial tensions under pressure and temperature conditions of CO2 geological storage. Energy Conversion and Management, **48**, 736-744. (2007)
5. S. Bachu, D. B. Bennion, Dependence of CO2-brine interfacial tension on aquifer pressure, temperature and water salinity. *Energy Procedia*, **1**, 3157-3164. (2009)
6. D.B. Bennion, S. Bachu, The impact of interfacial tension and pore size distribution/capillary pressure character on CO2 relative permeability at reservoir conditions in CO2-brine systems. In *SPE/DOE symposium on improved oil recovery.* OnePetro. (2006)
7. G. Kravanja, Ž. Knez, M. K. Hrnčič, The effect of argon contamination on interfacial tension, diffusion coefficients and storage capacity in carbon sequestration processes. *International Journal of Greenhouse Gas Control*, **71**, 142-154. (2018)
8. S. Saraji, L. Goual, M. Piri, H. Plancher, Wettability of supercritical carbon dioxide/water/quartz systems: Simultaneous measurement of contact angle and interfacial tension at reservoir conditions. *Langmuir*, **29**, 6856-6866. (2013)
9. S. Saraji, M. Piri, L. Goual, The effects of SO2 contamination, brine salinity, pressure, and temperature on dynamic contact angles and interfacial tension of supercritical CO2/brine/quartz systems. *International Journal of Greenhouse Gas Control*, **28**, 147 155. (2014)
10. M. Andrew, B. Bijeljic, M. J. Blunt, Pore-scale contact angle measurements at reservoir conditions using X-ray microtomography. *Advances in Water Resources*, **68**, 24-31. (2014)
11. P. Bikkina, I. Shaik, Interfacial tension and contact angle data relevant to carbon sequestration. *Carbon Capture, Utilization and Sequestration*, 163-186. (2018)
12. S. Schlüter, A. Sheppard, K. Brown, et al, 2014. Image Processing of Multiphase Images Obtained via X-ray Microtomography: A Review. *Water Resources Research*, **50** (4): 3615–3639.(2014) https://doi.org/10.1002/2014WR015256.
13. J. Dvorkin, N. Derzhi, M. Armbruster, et al., Method for Determining Permeability of Rock Formation Using Computer Tomographic Images Thereof. US Patent No. US8081802B2. (2008)
14. Y. Mu, R. Sungkorn, J. Toelke, J. Identifying the Representative Flow Unit for Capillary Dominated Two-Phase Flow in Porous Media Using Morphology-Based Pore-Scale Modeling. *Advances in Water Resources*, **95**: 16–28. (2016)
15. X. Nie, V. Gundepalli, Y. Mu, et al., Numerical Investigation of Oil-Water Drainage and Imbibition in Digitized Sandstones. *Mechanics & Industry*, **17** (2): Article 202. (2016)
16. A. Grader, K.A Birkedal, R. Engelman, K. Birkeland, N.A. Aarseth, Integrated Physical and Digital Chalk Relative Permeability Evaluation: A Case Study. *SPWLA*, (2023) https://doi.org/10.30632/SPWLA-2023-0028
17. R. Sedaghatinasab, S. Kord, J. Moghadasi, A. Soleymanzadeh Relative Permeability Hysteresis and Capillary Trapping during CO2 EOR and Sequestration. *International Journal of Greenhouse Gas Control*, Volume **106**, 1750-5836. (2021)

Appendix A: Counter Current Imbibition Data

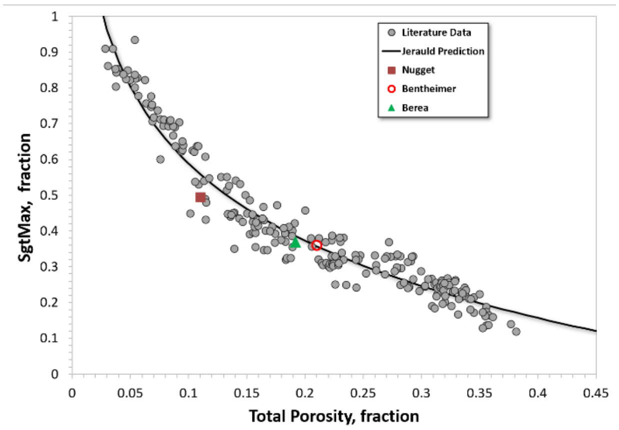

Figure A1: SgtMax (Max Trapped Gas Saturation) versus Total Porosity Fraction

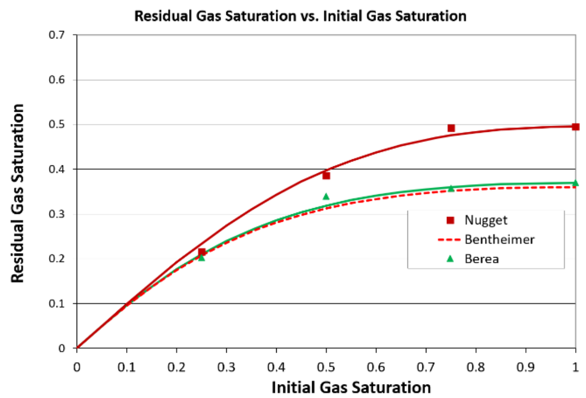

Figure A2: Residual Gas Saturation versus Initial Gas Saturation

Appendix B: Unsteady-State Primary Drainage Relative Permeability History Matching Evaluation

Appendix B.1 Nugget

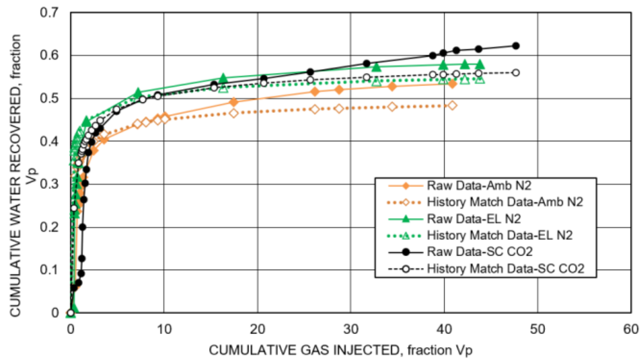

***Figure B1.1**: Nugget, Cumulative Water Recovery versus Cumulative Gas Injected History Match*

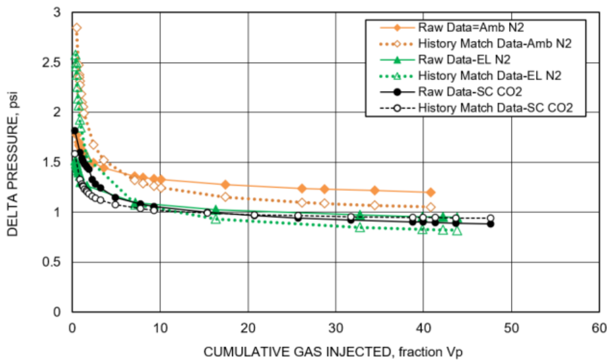

***Figure B1.2:** Nugget, Delta Pressure versus Cumulative Gas Injected History Match*

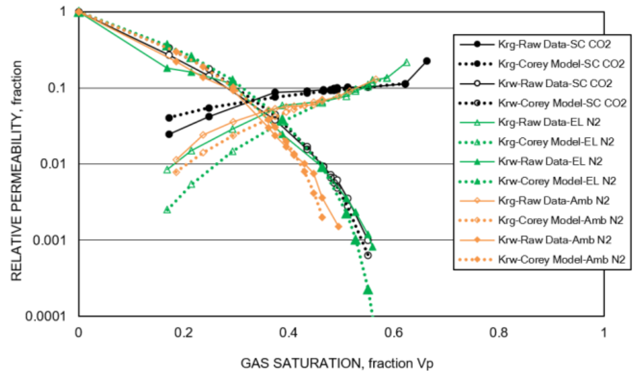

***Figure B1.3:** Nugget, Relative Permeability versus Gas Saturation History Match*

Appendix B.2 Bentheimer

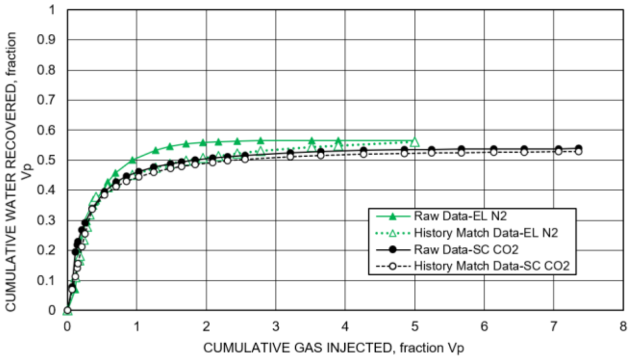

Figure B2.1*:Bentheimer, Cumulative Water Recovery versus Cumulative Gas Injected History Match*

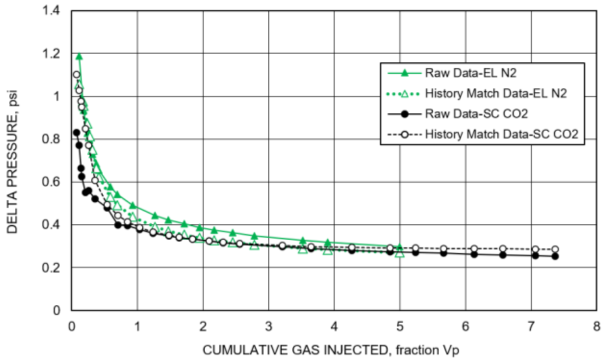

Figure B2.2: *Bentheimer, Delta Pressure versus Cumulative Gas Injected History Match*

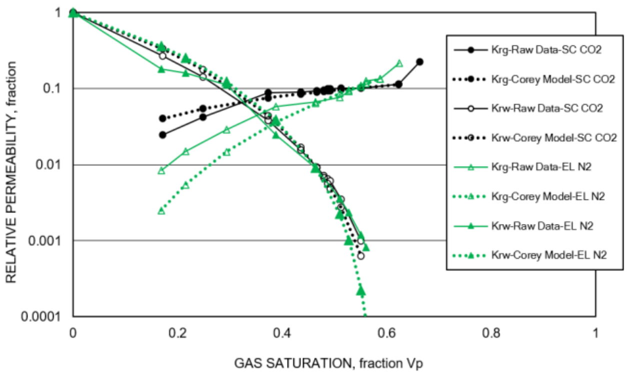

Figure B2.3: *Bentheimer, Relative Permeability versus Gas Saturation History Match*

Appendix B.3 Bandera

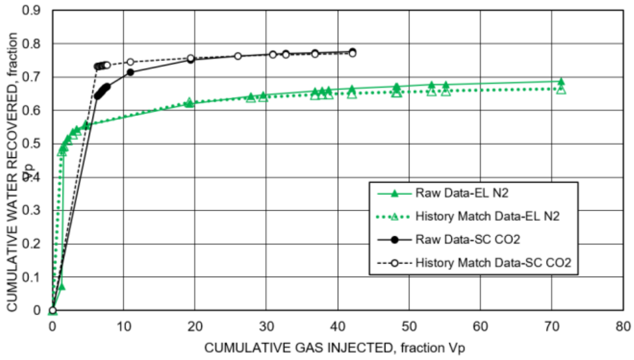

Figure B3.1: *Bandera, Cumulative Water Recovery versus Cumulative Gas Injected History Match*

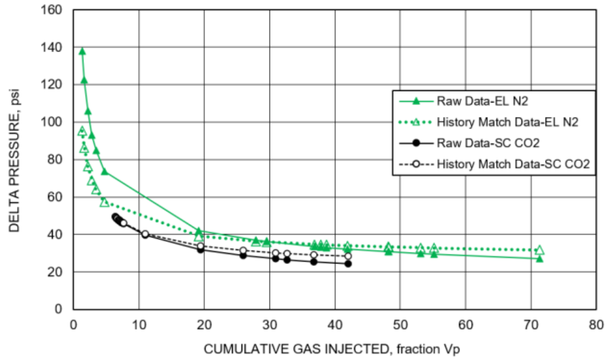

Figure B3.2: *Bandera, Delta Pressure versus Cumulative Gas Injected History Match*

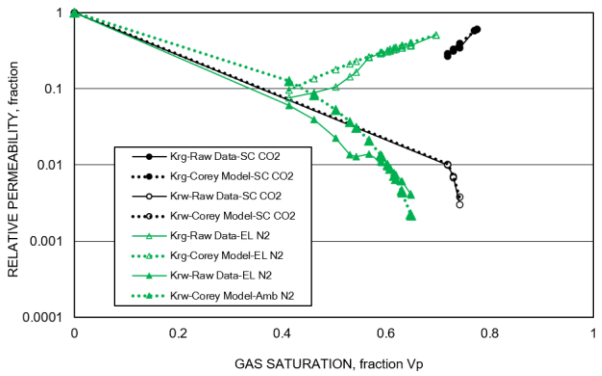

Figure B3.3*: Bandera, Relative Permeability versus Gas Saturation History Match*